https://doi.org/10.1093/plphys/kiac412 PLANT PHYSIOLOGY 2022: 190: 2706–2721

Plant Physiology®

Research Article

PHYTOCHROME-INTERACTING FACTOR 4/HEMERA-mediated thermosensory growth requires the Mediator subunit MED14

Abhishesh Bajracharya ,[1] Jing Xi ,[2] Karlie F. Grace,[1] Eden E. Bayer,[1] Chloe A. Grant,[1] Caroline H. Clutton ,[1] Scott R. Baerson ,[2] Ameeta K. Agarwal [3,4] and Yongjian Qiu [1,*]

1 Department of Biology, University of Mississippi, Oxford, Mississippi 38677, USA
2 Natural Products Utilization Research Unit, U.S. Department of Agriculture, Agricultural Research Service, Oxford, Mississippi, USA
3 National Center for Natural Products Research, School of Pharmacy, University of Mississippi, Oxford, Mississippi, USA
4 Division of Pharmacology, Department of BioMolecular Sciences, School of Pharmacy, University of Mississippi, Oxford, Mississippi, USA

*Author for correspondence: Yongjian Qiu (yqiu@olemiss.edu)

Y.Q. and A.B. conceived the original research plan; Y.Q., S.R.B., and A.K.A. supervised the experiments; A.B., J.X., K.F.G., E.E.B., C.A.G., C.H.C., A.K.A., and Y.Q. performed the experiments; A.B., J.X., S.R.B., A.K.A., and Y.Q. analyzed the data; Y.Q. wrote the article with the contributions from all authors; all authors approved the submitted version.

The author responsible for distribution of materials integral to the findings presented in this article in accordance with the policy described in the Instructions for Authors (https://academic.oup.com/plphys/pages/general-instructions) is: Yongjian Qiu (yqiu@olemiss.edu).

Abstract

While moderately elevated ambient temperatures do not trigger stress responses in plants, they do substantially stimulate the growth of specific organs through a process known as thermomorphogenesis. The basic helix–loop–helix transcription factor PHYTOCHROME-INTERACTING FACTOR 4 (PIF4) plays a central role in regulating thermomorphogenetic hypocotyl elongation in various plant species, including Arabidopsis (*Arabidopsis thaliana*). Although it is well known that PIF4 and its co-activator HEMERA (HMR) promote plant thermosensory growth by activating genes involved in the biosynthesis and signaling of the phytohormone auxin, the detailed molecular mechanism of such transcriptional activation is not clear. In this report, we investigated the role of the Mediator complex in the PIF4/HMR-mediated thermoresponsive gene expression. Through the characterization of various mutants of the Mediator complex, a tail subunit named MED14 was identified as an essential factor for thermomorphogenetic hypocotyl growth. MED14 was required for the thermal induction of PIF4 target genes but had a marginal effect on the levels of PIF4 and HMR. Further transcriptomic analyses confirmed that the expression of numerous PIF4/HMR-dependent, auxin-related genes required MED14 at warm temperatures. Moreover, PIF4 and HMR physically interacted with MED14 and both were indispensable for the association of MED14 with the promoters of these thermoresponsive genes. While PIF4 did not regulate MED14 levels, HMR was required for the transcript abundance of *MED14*. Taken together, these results unveil an important thermomorphogenetic mechanism, in which PIF4 and HMR recruit the Mediator complex to activate auxin-related growth-promoting genes when plants sense moderate increases in ambient temperature.

Received June 28, 2022. Accepted August 12, 2022. Advance access publication September 5, 2022

Introduction

Plants are highly sensitive to environmental temperature changes. Moderately elevated ambient temperatures below heat shock (between 12°C and 27°C) do not trigger stress responses, but they may drastically alter plant growth and development, including rapid stem and root elongation, enhanced petiole hyponastic growth, early flowering, and reduced stomatal index. Collectively, these responses are referred to as thermomorphogenesis (Casal and Balasubramanian, 2019; Ludwig et al., 2021; Park et al., 2021).

Thermomorphogenetic responses, such as thermosensory hypocotyl elongation, involve massive transcriptomic reprogramming, as demonstrated in the model dicotyledonous plant Arabidopsis (*Arabidopsis thaliana*; Liu and Charng, 2013; Sidaway-Lee et al., 2014; Cortijo et al., 2017; Ding et al., 2018; Han et al., 2019; Bordiya et al., 2020; Jin et al., 2020; Lee et al., 2020, 2021b, 2021c). A major effect of this transcriptomic reprogramming is to activate genes involved in auxin synthesis, such as *YUCCA8* (*YUC8*), and auxin signaling, such as *INDOLE-3-ACETIC ACID INDUCIBLE 19* and *29* (*IAA19* and *IAA29*; Franklin et al., 2011; Sun et al., 2012; Ma et al., 2016; Zhu et al., 2016). PHYTOCHROME-INTERACTING FACTOR 4 (PIF4), a central transcriptional regulator of thermomorphogenesis (Qiu, 2020), activates these auxin-related genes in response to warm temperatures (Franklin et al., 2011; Sun et al., 2012; Ma et al., 2016; Zhu et al., 2016). PIF4 belongs to an eight-member basic helix–loop–helix (bHLH) transcription factor family, which was originally identified as a key player in transducing light signals perceived by the red/far-red (R/FR) photoreceptors known as phytochromes (Leivar and Quail, 2011). PIFs are integrators of light and various environmental and developmental signals (Leivar and Quail, 2011; Leivar and Monte, 2014; Pham et al., 2018). Although PIFs show apparent functional redundancy in multiple morphogenetic responses (Leivar and Monte, 2014; Pham et al., 2018), thermomorphogenesis is mediated primarily through PIF4 (Koini et al., 2009; Stavang et al., 2009; Kumar et al., 2012; Qiu et al., 2019). As an early ambient temperature signaling component, PIF4 is regulated at multiple levels, including transcription, post-translational modification, DNA-binding affinity, transcriptional activity, and protein stability (Qiu, 2020). Recent reports revealed distinct temperature-signaling mechanisms under different light conditions or photoperiod regimes, indicating more complex regulation of PIF4-mediated thermal responses by light quality, day length, and the circadian clock (Box et al., 2015; Park et al., 2017; Qiu et al., 2019).

Besides its role in thermomorphogenesis, PIF4 also activates growth-promoting genes during skotomorphogenesis (growth in darkness) and shade-avoidance responses (Leivar and Monte, 2014). PIF4 possesses a transactivation domain (TAD) that resembles that of PIF3 (Dalton et al., 2016; Yoo et al., 2021). The tomato PIF4 activates shade-induced genes by interacting with MED25, a tail component of the Mediator complex (Sun et al., 2020). These data suggest that PIF4 has a functional TAD that promotes shade-avoidance responses. However, whether PIF4's TAD is equally important for its activity in thermomorphogenesis is unknown. We previously demonstrated that PIF4-mediated thermomorphogenetic control of growth-promoting gene expression requires the transcriptional coactivator HEMERA (HMR; Qiu et al., 2019). HMR physically interacts with PIF4 and activates the thermo-inducible PIF4 target genes through an acidic nine-amino-acid transactivation domain (9aaTAD). A weak allele named *hmr-22* harbors a D516N mutation in the 9aaTAD, largely disrupting HMR's transactivation activity and leading to defects in the thermosensory growth (Qiu et al., 2015, 2019). Mechanistic insights into the function of HMR's TAD in regulating PIF4 activity have yet to be revealed.

HMR's 9aaTAD resembles the TADs present in prototypic acidic transcription activators, such as Viral Protein 16 (VP16), Galactose 4 (GAL4), General Control Nonderepressible 4 (GCN4), and Myelocytomatosis (MYC; Piskacek et al., 2007). These acidic TADs interact directly with subunits of the Mediator complex to facilitate the assembly or the stability of the RNA polymerase II (Pol II) preinitiation complex (PIC) at the transcriptional initiation site (Borggrefe and Yue, 2011; Vojnic et al., 2011). The Mediator complex is a multisubunit transcriptional coordinator that transmits signals from transcription activators to the Pol II preinitiation transcription activators and is required for the transcription of virtually all Pol II-transcribed genes (Dolan et al., 2017).

Much of our current understanding of the three-dimensional structure of the Mediator complex has come from studies performed on yeast and mammals (Robinson et al., 2016; Nozawa et al., 2017; Schilbach et al., 2017; Tsai et al., 2017; Chen et al., 2021; Rengachari et al., 2021). Despite the low sequence similarity between some Arabidopsis Mediator subunits and those of yeast and metazoans, more than 20 Mediator subunits are conserved across yeast, plants, and metazoans (Bourbon, 2008). Furthermore, the Mediator complexes in all three kingdoms share a generally similar modular composition, with subunits organized into head, middle, tail, and kinase subcomplexes (Malik and Roeder, 2010; Buendía-Monreal and Gillmor, 2016; Dolan and Chapple, 2017). The head and middle modules form the essential core Mediator that directly interacts with PIC (Nozawa et al., 2017; Schilbach et al., 2017). PIC-Mediator assembly further creates a Head-Middle sandwich to stabilize two Pol II C-terminal domain (CTD) segments and position CTD for phosphorylation (Chen et al., 2021). In contrast to the head and middle subunits, the subunits of the tail module are relatively loosely associated with each other and are targeted by activators and repressors (Malik and Roeder, 2010; Cevher et al., 2014; Zhao et al., 2021).

To further elucidate the molecular mechanism by which PIF4 and HMR recruit the transcriptional machinery when activating the expression of thermoresponsive genes, we performed a reverse genetic screen for Arabidopsis Mediator

mutants that show reduced sensitivity to moderate temperature elevations. Here, we report the identification of MED14 as a key subunit of the Mediator complex that is recruited by PIF4 and HMR to activate auxin-related, growth-promoting genes in response to warm temperatures.

Results

MED14 is required for thermosensory hypocotyl growth

To investigate the role of the Mediator complex in thermomorphogenesis and search for Mediator subunits that work with PIF4 and HMR to induce the transcription of thermoresponsive genes, we first tested the thermal sensitivity of mutants of various Mediator subunits in continuous red (R) light. Most mutants of the Mediator subunits in the head, middle, and kinase modules showed similar responses to the warm temperature as wild-type—the ratio of hypocotyl length between 27°C and 20°C was comparable with those in the wild-type seedlings (Supplemental Figure S1). In comparison, mutants of several tail subunits, including MED14, MED16, and MED25, were hyposensitive to the increased temperature (Figure 1, A–C). The ratios of hypocotyl length at 27°C to that at 20°C in *med14* (SAIL_373_C07), *med16-2* (SALK_048091), *med16-3* (WISCDSLOX504A08), *med25-2* (SALK_129555C), and *med25-3* (SALK_059316C) were significantly lower than those of wild-type seedlings (Figure 1C). Among these mutants, *med14* showed the most dramatic reduction in thermomorphogenetic hypocotyl growth—it had only 37% of the wild-type thermal response and ∼70% of the wild-type hypocotyl length at 27°C. Besides, *med14* also showed a much shorter petiole length and smaller petiole angles than the wild-type at 27°C, indicative of two other thermomorphogenetic defects in petiole elongation and leaf hyponastic response (Figure 1D; Supplemental Figure S2).

The *med14* mutant (SAIL_373_C07) was the only viable T-DNA insertion line with dramatically reduced *MED14* expression (Zhang et al., 2013). To further confirm that the thermomorphogenetic defect of *med14* was caused by decreased *MED14* levels, we generated *MED14* overexpression lines in the *med14* mutant background. A full-length *MED14* CDS driven by the 35S Cauliflower Mosaic Virus (CaMV) constitutive promoter was expressed with a C-terminal human influenza hemagglutinin (HA) tag. The resulting transgenic plants, designated *35S::MED14–HA/med14*, successfully complemented the morphological phenotype of *med14* at 27°C and largely rescued its reduced sensitivity in thermomorphogenetic hypocotyl growth (Figure 1, D–F). Moreover, the transgene also completely recovered the thermo-induced petiole elongation and substantially restored the leaf hyponastic response of *med14* (Figure 1D; Supplemental Figure S2). These data further support that MED14 plays a crucial role in Arabidopsis thermomorphogenesis.

It is worth noting that *med14*'s defect in thermomorphogenesis was not limited to the continuous R light condition. When grown in continuous white light, the *med14* mutant was almost completely insensitive to the warmer temperature—while the wild-type seedlings showed a 2.8-fold increase in hypocotyl length between 27°C and 20°C, only a 1.1-fold increase was observed in *med14* (Supplemental Figure S3). These phenotypes highly resembled those of *pif4-2* and *hmr-22* mutants in the same condition, which motivated us to further investigate the relationship between MED14 and PIF4/HMR in thermomorphogenesis.

MED14 regulates the thermal induction of key auxin-related PIF4 targets

PIF4 and HMR promote thermosensory hypocotyl growth by activating key genes in auxin biosynthesis (e.g. *YUC8*) and signaling (e.g. *IAA19* and *IAA29*). The identification of MED14's role in thermomorphogenesis prompted us to test whether MED14 is the tail component that works with PIF4 and HMR in activating the expression of these growth-related, thermo-induced genes. Toward this end, we first examined the steady-state transcript levels of *YUC8*, *IAA19*, and *IAA29* in 4-day-old Col-0 and *med14* seedlings grown at lower and warmer temperatures. While the transcription of all three genes was stimulated at 27°C in Col-0, these increases were not observed in *med14* (Figure 2A). Similarly, a 6-h warm temperature treatment greatly induced the expression levels of all three markers in Col-0, but not in the *med14* mutant (Figure 2B).

Given that the Mediator complex is essential for all Pol II-mediated transcription (Jeronimo and Robert, 2017; Soutourina, 2018) and that MED14 is a key component of the Mediator complex (Buendía-Monreal and Gillmor, 2016; Yang et al., 2016), the hypomorphic mutation in *med14* might also affect the expression of *PIF4* and *HMR*. Indeed, the absolute transcript levels of *HMR* and *PIF4* in the *med14* mutant were lower than those in Col-0 at 27°C (Figure 2A). In addition, the thermo-induced *PIF4* expression was also compromised in *med14* (Figure 2B). To evaluate whether the decreases in *HMR* and *PIF4* transcript levels resulted in lower protein abundance in *med14*, we performed immunoblots with four biological replicates to compare the change of HMR and PIF4 protein levels between Col-0 and *med14* in response to thermal treatment (Supplemental Figure S4). In a couple of replicates, we did observe slightly lower HMR protein levels in the *med14* mutant than in Col-0 at each time point after the 20°C–27°C transition (Supplemental Figure S4, B and D). However, these differences were not statistically significant after assessing all four replicates ($P > 0.05$; Figure 2C; Supplemental Figure S4E). The peak PIF4 protein level (8 h after thermal treatment) was significantly reduced in the *med14* mutant when compared with Col-0 (Figure 2C). However, we could still observe a notable increase in PIF4 protein levels in *med14* after the 20°C–27°C transition (Figure 2C; Supplemental Figure S4). These data imply that MED14 might contribute to the thermoresponsive expression of the PIF4/HMR-regulated genes (*YUC8*, *IAA19*, and *IAA29*) in two ways—a direct role by assisting PIF4's and HMR's transactivation activity and an indirect

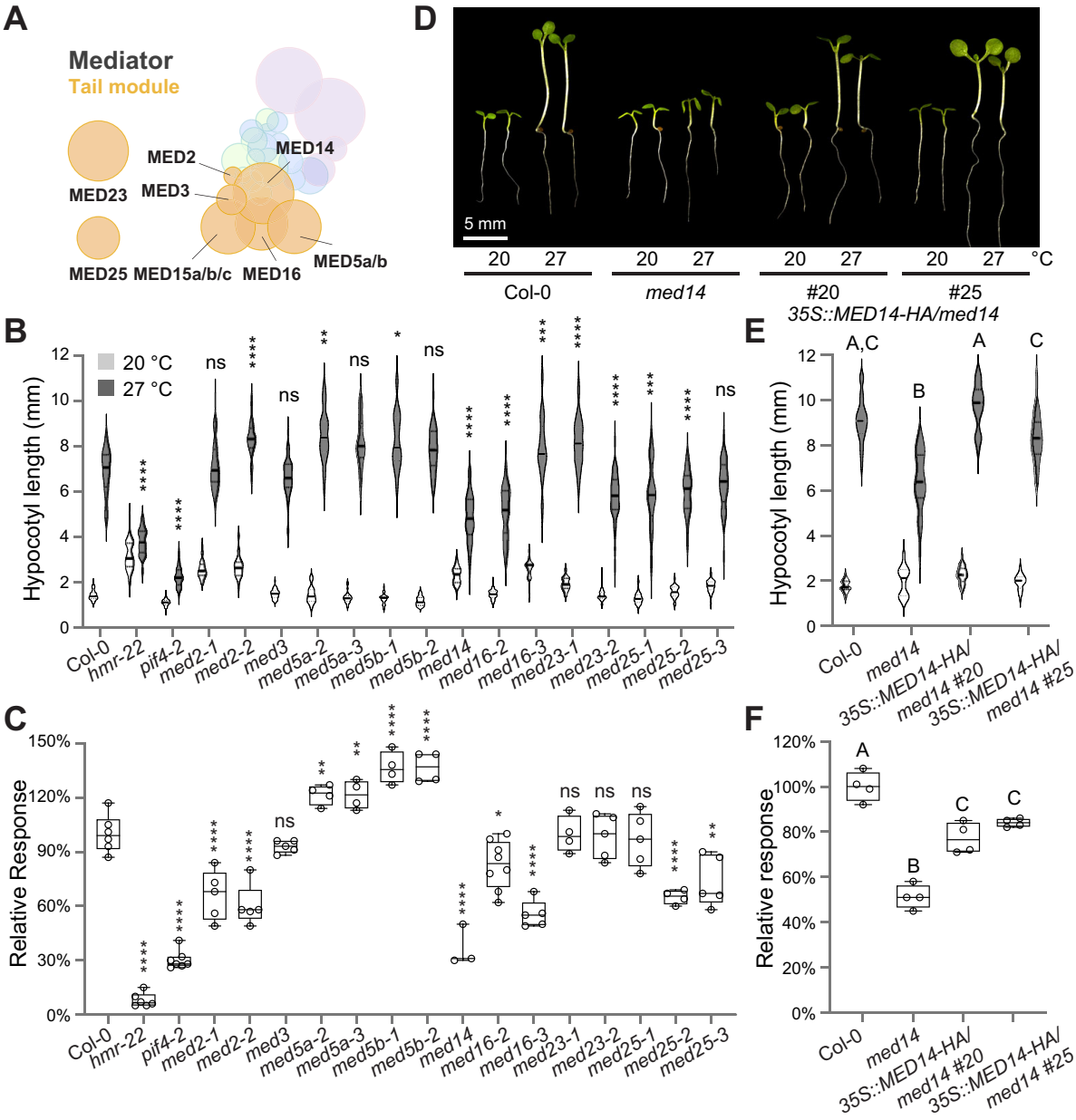

Figure 1 MED14 is a crucial regulator of thermomorphogenesis. A, Schematic illustration of the Arabidopsis Mediator complex, with an emphasis on components in the tail module. The size of each circle reflects the relative protein size (predicted molecular weight) of each Mediator subunit. The relative position of each Mediator component is based on the cryo-EM and crystal structures of yeast and human Mediator shown by Tsai et al., 2014 and Robinson et al., 2015 and interaction data of Arabidopsis Mediator subunits shown by Maji et al., 2019. Note that the positions of MED23 and MED25 in the tail module are undetermined. Protein subunits in each module are colored in different colors: head module, green; middle module, blue; tail module, orange; cyclin kinase module, purple. See supplemental data for clear compositions of each module. B, Hypocotyl length measurements of mutant seedlings of Mediator tail subunits. Seedlings were grown for 4 days in continuous red (R) light (50 μmol m^{-2} s^{-1}). The white and grey violin plots represent hypocotyl length measurements at 20°C and 27°C, respectively. The elements of violin plots are as follows: solid line, median; lower dotted line, first quartile; upper dotted line, third quartile. The results of the one-way ANOVA analysis comparing the absolute hypocotyl length between Col-0 and each mutant grown at 27°C are shown ($n > 30$). $^{****}P < 0.0001$; $^{***}P < 0.001$; $^{**}P < 0.01$; $^{*}P < 0.05$; ns, not significant ($P \geqslant 0.05$). C, Comparison of the relative thermal response among the seedlings in (B). The elements of box plots are as follows: center line, median; box limits, first and third quartiles; whiskers, minimum and maximum values; points, all data points. The relative response is defined as the relative hypocotyl response to 27°C of a mutant compared with that of Col-0 (which is set at 100%). The results of the one-way ANOVA analysis comparing the relative response between Col-0 and each mutant are shown ($n \geqslant 3$). $^{****}P < 0.0001$; $^{***}P < 0.001$; $^{**}P < 0.01$; $^{*}P < 0.05$; ns, not significant ($P \geqslant 0.05$). D, Representative images of 4-d-old Col-0, *med14*, and *35S::MED14–HA/med14* (#20 and #25) seedlings in continuous R light (50 μmol m^{-2} s^{-1}) at either 20°C or 27°C. Images of seedlings grown in different conditions were digitally extracted and assembled for easy comparison. All the images were acquired using a Leica MZ10 F modular stereo microscope with the same settings (e.g. light, focus, and magnification). Scale bar, 5 mm. E, Hypocotyl length measurements of seedlings in (D). The elements of violin plots are the same as in (B). Different letters denote significant statistical differences between the absolute hypocotyl length of each line grown at 27°C (one-way ANOVA, $n > 30$, $P < 0.0001$). F, Comparison of the relative thermal response among the seedlings in (D). The elements of box plots are the same as in (C). Different letters denote significant statistical differences between the relative response of each line (one-way ANOVA, $n \geqslant 4$, $P < 0.0001$).

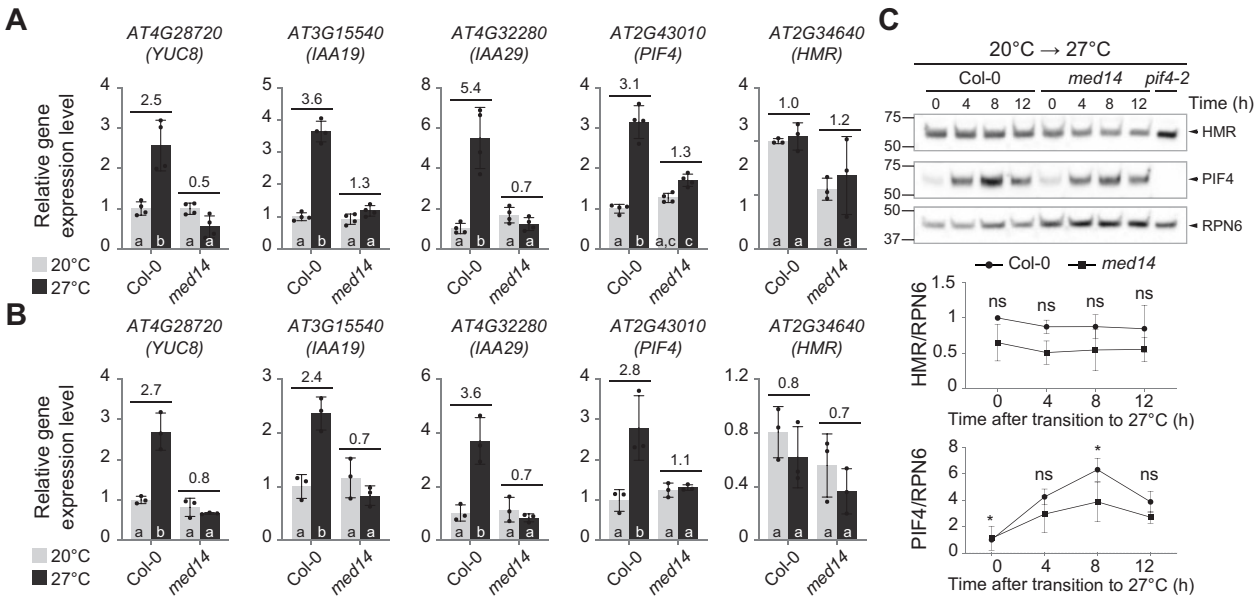

Figure 2 MED14 is required for the thermo-induced expression of PIF4 target genes. A, RT–qPCR analysis of the steady-state transcript levels of *YUC8*, *IAA19*, *IAA29*, *PIF4*, and *HMR* in Col-0 and *med14* seedlings grown in continuous red (R) light (50 μmol m^{-2} s^{-1}) for 96 h at 20°C and 27°C. Different lowercase letters at the bottom of bars denote significant statistical differences between the relative gene expression level (two-way ANOVA with Tukey HSD, $n = 4$ or 3, $P < 0.001$ for *YUC8*, *IAA29*, $P < 0.0001$ for *IAA19*, $P < 0.01$ for *PIF4*, and $P < 0.05$ for *HMR*). Numbers indicate the fold changes between transcript levels at these two temperatures. Error bars represent the SD of three or four biological replicates. B, RT–qPCR analysis of the steady-state transcript levels of *YUC8*, *IAA19*, *IAA29*, *PIF4*, and *HMR* in Col-0 and *med14* during the 21°C–27°C transitions. Seedlings were grown in continuous R light (50 μmol m^{-2} s^{-1}) for 96 h and then transferred to 27°C in the same light condition. Samples were taken before (light gray) and 6 h after (dark gray) the 27°C treatment. Different lowercase letters at the bottom of bars denote significant statistical differences between the relative gene expression level (two-way ANOVA with Tukey HSD, $n = 3$, $P < 0.001$ for *YUC8*, $P < 0.01$ for *IAA19*, *IAA29*, $P < 0.05$ for *PIF4*, and not significant for *HMR*). Fold changes in the transcript levels by the 27°C treatment are shown above the columns. In both (A) and (B), *PP2A* was used as an internal control. For each gene, the transcript level in Col-0 at 20°C was set to 1, and others were calculated by the $2^{-\Delta\Delta Ct}$ method. Error bars represent the SD of three or four biological replicates. C, Immunoblot analysis of HMR and PIF4 levels in Col-0 and *med14* during the 20°C–27°C transitions. Seedlings were grown in continuous R light (50 μmol m^{-2} s^{-1}) for 96 h and then transferred to 27°C in the same light condition. Samples were collected and analyzed at the indicated time points. RPN6 was used as a loading control. The relative levels of HMR and PIF4, normalized to RPN6, are shown underneath the immunoblots. The normalized level (HMR/RPN6 or PIF4/RPN6) in Col-0 at 20°C before transition (time 0 h) was set to 1 and others were calculated as relative levels. The results of the Student's *t* test analysis are shown ($n = 4$). $^{*}P < 0.05$; ns, not significant ($P \geq 0.05$). The immunoblots of all four biological replicates are shown in supplemental data.

role by modulating the *PIF4* transcript level when plants are exposed to warmer temperatures. It is currently difficult to evaluate the exact contribution of each role to PIF4/HMR-mediated thermomorphogenetic gene expression.

MED14, HMR, and PIF4 co-regulate a subset of thermoresponsive genes

Previous transcriptomic analyses by other groups have shown that 4%–16% of Arabidopsis genes are differentially regulated by warm temperatures and the expression of a large portion of these thermoregulated genes requires PIF4 (Ding et al., 2018; Jin et al., 2020; Kim et al., 2020; Lee et al., 2020, 2021b, 2021c). The observation that MED14 is indispensable for the thermal induction of several essential PIF4/HMR target genes motivated us to further explore its connection with PIF4 and HMR in controlling the thermoresponsive gene expression on the genome-wide scale. Therefore, we performed RNA-sequencing (RNA-seq) on 4-day-old Col-0, *pif4-2*, *hmr-22*, and *med14* seedlings grown at 20°C and 27°C under continuous R light.

When comparing expression levels at 27°C with those at 20°C, 828 and 938 genes were induced and repressed at least two-fold by warmer temperature in Col-0 (false discovery rate [FDR]-adjusted $P < 0.001$, Fragments Per Kilobase of exon per Million reads mapped [FPKM] > 1), respectively (Figure 3A; Supplemental Data Set 1). These results are in agreement with previous studies in which similar growth conditions were used (Lee et al., 2020, 2021c). For example, 483 of 828 thermo-induced genes (58%) and 550 out of 938 (59%) thermo-repressed genes in the current study overlapped with at least one study reported by Lee et al. (2020, 2021b) (Supplemental Figure S5; Supplemental Data Set 2). The *pif4-2*, *hmr-22*, and *med14* mutants displayed distinct transcriptome profiles compared with Col-0 and a large proportion of genes were uniquely induced or repressed at 27°C in each mutant (Figure 3A; Supplemental Data Set 1). Even though several genes were also shared between Col-0

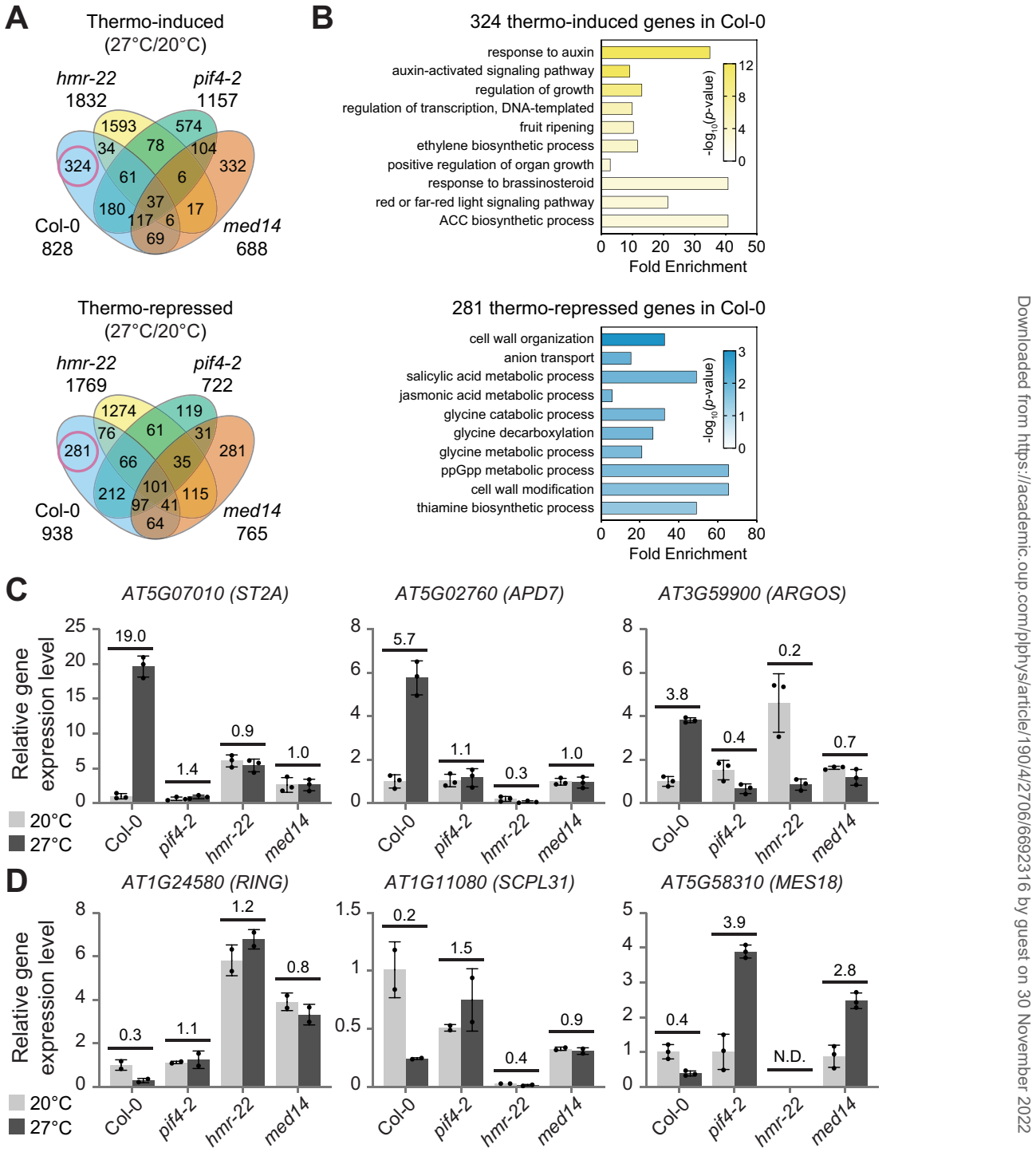

Figure 3 Thermo-induced expression of a group of auxin-related, growth-promoting genes requires PIF4, HMR, and MED14. A, A Venn diagram shows unique and co-regulated thermo-induced and thermo-repressed genes in wild-type (Col-0), *pif4-2*, *hmr-22*, and *med14* mutants. The red circles indicate PIF4/HMR/MED14-dependent genes that were uniquely induced and repressed in Col-0 but not in the mutants at 27°C. Seedlings were grown in continuous red (R) light (50 μmol m^{-2} s^{-1}) for 96 h at either 20°C or 27°C, and total RNA was extracted from four biological replicates for RNA-seq analyses. B, Gene ontology analysis of the 324 PIF4/HMR/MED14-dependent thermo-induced genes and 281 PIF4/HMR/MED14-dependent thermo-repressed genes. The bar represents the fold enrichment and the color indicates the $-\log_{10}$ (*P*-value). The fold enrichment score is defined by the GeneCodis 4 software as the ratio between two fractions: the number of query genes in the GO term/the total number of query genes as the numerator, and the number of total genes in the GO term/the total number of Arabidopsis genes as the denominator. ACC, 1-aminocyclopropane-1-carboxylate (an ethylene precursor). ppGpp, guanosine tetraphosphate. C and D, RT–qPCR analysis of representative PIF4/HMR/MED14-dependent genes in Col-0, *pif4-2*, *hmr-22*, and *med14*. Total RNA was extracted from seedlings grown in continuous R light (50 μmol m^{-2} s^{-1}) for 96 h at either 20°C or 27°C. The relative expression of three thermo-induced (C) and three thermo-repressed genes (D) were normalized to the expression level of *PP2A* after RT–qPCR. For each gene, the transcript level in Col-0 at 20°C was set to 1, and others were calculated by the $2^{-\Delta\Delta Ct}$ method. Error bars represent the SD of two (*RING* and *SCPL31*) or three (*ST2A*, *APD7*, *ARGOS*, and *MES18*) biological replicates. Numbers indicate the fold changes between transcript levels at these two temperatures. ND, not detected.

and each mutant, 324 and 281 SSTF genes were uniquely induced and repressed in Col-0 at 27°C, respectively (Figure 3A; Supplemental Figure S6A and Supplemental Data Set 3). We, therefore, named these genes PIF4/HMR/MED14-dependent thermo-induced and thermo-repressed genes. We performed gene ontology (GO) analysis on these two groups of thermo-regulated genes. Notably, many genes involved in growth-related phytohormone signaling (e.g. auxin, brassinosteroid, and ethylene) were upregulated in Col-0 but not in these three mutants, and a number of genes involved in cell wall organization and modification were downregulated only in Col-0 (Figure 3B). This observation is consistent with the thermomorphogenetic hypocotyl growth phenotype of these genotypes (Figure 1, B and C).

To evaluate whether these PIF4/HMR/MED14-dependent thermoresponsive genes are directly or indirectly regulated by PIF4, we compared our datasets with published PIF4-associated genes from three studies (Supplemental Data Set 4). Possibly due to different growth conditions and treatment methods, the number of PIF4-binding genes identified through chromatin immunoprecipitation sequencing (ChIP-seq) assays in the three studies varied from approximately 1,000 to over 7,000 (Oh et al., 2012; Pfeiffer et al., 2014; Pedmale et al., 2016). We defined the thermo-regulated PIF4 direct targets as the PIF4/HMR/MED14-dependent thermoresponsive genes that were identified in at least two of the three published studies. While $<10\%$ of the thermo-repressed genes (25 out of 281) were associated with PIF4, about one-third of the thermo-induced genes (114 out of 324) are PIF4 direct targets (Supplemental Figure S6B and Supplemental Data Set 4). Therefore, MED14 may mainly function as a coactivator, rather than a repressor, in regulating thermoresponsive PIF4 targets. GO analyses of these two datasets showed similar results as those of PIF4/HMR/MED14-dependent thermoresponsive genes (Supplemental Figure S6C). Many auxin-responsive genes, including *IAA19*, *IAA29*, and a group of *SMALL AUXIN UP RNA* (*SAUR*) genes, were enriched in the PIF4/HMR/MED14-dependent thermo-induced PIF4 targets; several genes involved in cell wall modification and lignin metabolic process were enriched in PIF4/HMR/MED14-dependent thermo-repressed PIF4 targets (Supplemental Figure S6C).

We further performed reverse transcription–quantitative polymerase chain reaction (RT–qPCR) analyses to confirm the RNA-seq results (Figure 3, C and D). The expression of three PIF4/HMR/MED14-dependent thermo-induced genes, *ST2A* (AT5G07010), *APD7* (AT5G02760), and *ARGOS* (AT3G59900), were highly induced in Col-0 at 27°C but remained the same or even decreased at 27°C in *pif4-2*, *hmr-22*, and *med14* mutants (Figure 3C). The expression of three PIF4/HMR/MED14-dependent thermo-repressed genes, *RING* (AT1G24580), *SCPL31* (AT1G11080), and *MES18* (AT5G58310), were greatly reduced in Col-0 at 27°C but not in those three mutants (Figure 3D). Taken together, these data suggest that MED14 co-regulates a group of growth-related, thermoresponsive genes with PIF4 and HMR.

PIF4 and HMR physically interact with MED14

The thermomorphogenetic defect of *med14* and the requirement of MED14 for the thermal induction of many PIF4 direct targets suggest that it may be the Mediator tail subunit that communicates with PIF4 and/or HMR during the transcriptional activation of those thermoresponsive genes. To test this hypothesis, we investigated the interactions between MED14 and PIF4/HMR. We first expressed PIF4 and HMR as glutathione S-transferase (GST) fusion proteins in *Escherichia coli* and used them as baits to test their interactions with in vitro transcribed/translated HA-MED14. Both GST-HMR and GST-PIF4 appear to interact strongly with HA-MED14 (Figure 4A).

We further confirmed the interactions between PIF4 and MED14 using bimolecular fluorescence complementation (BiFC) assays. When co-expressed with cyan fluorescent protein (CFP) in *Nicotiana benthamiana*, PIF4-NmVen210 interacted with MED14-cVen210 in about 30% (8 out of 23) of transformed nuclei as indicated by the colocalization of CFP and mVenus signals in the same nucleus (Figure 4B). In contrast, no mVenus signal was detected in any CFP-expressing nucleus (0 out of 31) when PIF4-NmVen210 was expressed with cVen210 alone (Figure 4B). We did not observe the yellow fluorescent signal when co-expressing HMR-NmVen210 and MED14-cVen210, which was probably because HMR is a nuclear/plastidial dual-localized protein, and its strong plastid transit peptide limits the abundance of HMR proteins in the nucleus (Chen et al., 2010; Nevarez et al., 2017). The difficulty of transiently expressing large-size proteins like MED14 (more than 1,700 amino acids) might also contribute to the low detection efficiency. Taken together, the results from the GST pull-down assays and the BiFC assays indicate that MED14 may be physically associated with PIF4 and HMR.

The association of MED14 with thermo-induced genes requires PIF4 and HMR

To elucidate the molecular mechanisms by which PIF4 and HMR recruit MED14 to the thermoresponsive PIF4 targets for transcriptional activation, we decided to compare the association of MED14 with representative PIF4 targets in the presence and absence of functional PIF4 or HMR using ChIP-qPCR assays. We crossed the *35S::MED14–HA/med14* transgenic line (#20) with *pif4-2* and *hmr-22*, respectively, and used the homozygous F3 progenies of *MED14–HA/pif4-2* and *MED14–HA/hmr-22* for following experiments. Like *pif4-2* and *hmr-22*, both *MED14–HA/pif4-2* and *MED14–HA/hmr-22* seedlings showed markedly reduced thermomorphogenetic hypocotyl growth (Supplemental Figure S7, A and B), suggesting that the proper transgene function and/or expression requires functional PIF4 and HMR.

Both *MED14–HA/pif4-2* and *MED14–HA/hmr-22* seedlings were further used to compare MED14 occupancy across *IAA29* and *IAA19*, two PIF4/HMR/MED14-dependent thermoresponsive PIF4 direct targets, with that in *MED14–HA* after a 6-h warm temperature treatment. The ChIP-qPCR results showed that MED14–HA is specifically associated

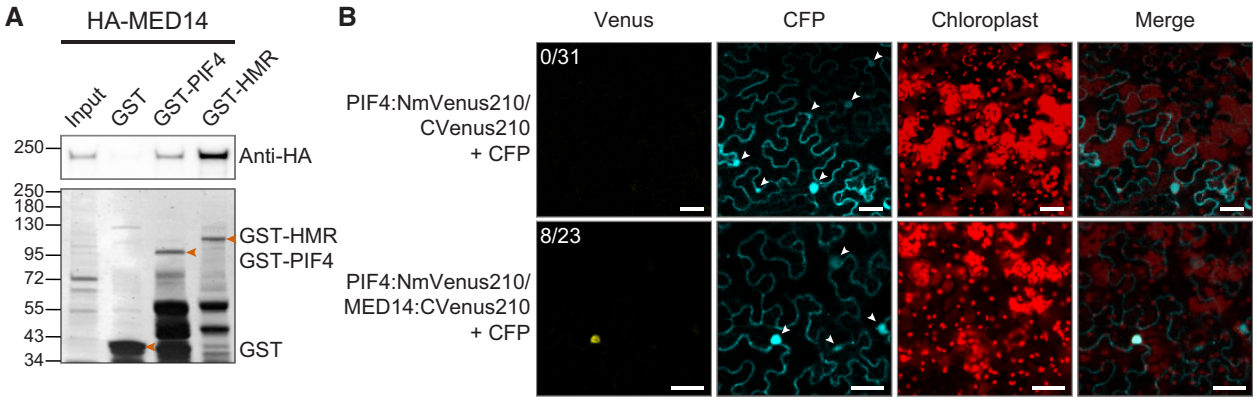

Figure 4 MED14 physically interacts with PIF4 and HMR. (A) GST pull-down assays. GST-tagged full-length PIF4 and HMR were used as baits to pull down in vitro translated HA-tagged MED14. The upper panel is an immunoblot using anti-HA antibodies showing the bound and input fractions of HA-MED14; the lower part is a Coomassie Blue-stained SDS–PAGE gel showing immobilized GST and GST-tagged PIF4 and HMR. B, Bimolecular fluorescence complementation assays. PIF4 fused with NmVenus210 (PIF4:NmVenus210) and MED14 fused with cVenus210 (MED14:CVenus210) were co-expressed in *N. benthamiana* through agroinfiltration. PIF4:NmVenus210 and CVenus210 were co-expressed as a control. The CFP was expressed simultaneously through agroinfiltration to indicate the locations of nuclei. The optical density of each *Agrobacterium* strain was 0.1 and images were captured 40–70 h after infiltration. White arrowheads indicate nuclei identified in the CFP channel. The nuclear fluorescence signal in the Venus channel indicates the interactions between the two proteins tested in each agroinfiltration. The number of nuclei showing the Venus signal out of the number of nuclei with the CFP signal is shown in the upper left corner of each Venus channel. The chloroplast channel is to show that the Venus signal was not caused by the chlorophyll autofluorescence. Scale bars, 40 μm.

with the G-box (CACGTG)-containing regions in both *IAA29* and *IAA19*, confirming the physical presence of MED14 in the promoters of these two PIF4 targets (Figure 5, A and B). Interestingly, this association was significantly reduced in the G-box-containing regions in the *pif4-2* or *hmr-22* mutant background (Figure 5, A and B; Supplemental Figure S8). We concomitantly assessed the MED14–HA protein levels in these lines. Knocking out *PIF4* did not affect the MED14–HA protein level, both before and after thermal treatment (Supplemental Figure S7, C and D), suggesting that the reduced MED14–HA binding to PIF4 targets in the *pif4-2* background was not caused by decreased MED14–HA abundance. In contrast, the MED14–HA protein level was dramatically lessened in the *hmr-22* background (Supplemental Figure S7, C and D). Moreover, the thermo-induced PIF4 accumulation was also abolished in *MED14–HA/hmr-22* (Supplemental Figure S7C), consistent with our previous studies (Qiu et al., 2019). Therefore, the declined association of MED14–HA with PIF4 target genes in the *hmr-22* background may be the consequence of the reduction in both MED14–HA and PIF4 protein levels.

We further investigated whether the reduced MED14–HA protein level in *MED14–HA/hmr-22* was caused by a decrease in the *MED14–HA* transcript level. The RT–qPCR results showed that although *MED14* was overexpressed in the *MED14–HA* line when compared with Col-0, this overexpression was abolished in the *hmr-22* background (Supplemental Figure S7E). While this experiment was performed using 4-day-old 20°C-grown seedlings treated at 27°C for 6 h, similar results were seen in 4-day-old *hmr-22* mutant grown at 20°C from our RNA-seq data (Supplemental Figure S7F). On the other hand, the *MED14* transcript levels were comparable in Col-0 and *hmr-22* grown at 27°C for 4 days. These data suggest that at lower ambient temperatures or even with short-term warm-temperature treatment, HMR is required for the RNA abundance of *MED14*, while long-term thermal treatment would partially rescue the *MED14* transcript level in the *hmr-22* background. In summary, these data indicate that MED14 may be recruited by PIF4 to the promoters of growth-related PIF4 targets for their thermo-induced expression, while HMR helps maintain high levels of MED14 and PIF4 at warm temperatures.

Discussion

Transcriptional regulation of thermoresponsive genes is one of the earliest and principal steps in plant thermomorphogenesis. We previously discovered that PIF4 and its coactivator HMR promote thermomorphogenetic hypocotyl growth in the daytime by activating the transcription of key growth-promoting genes (Qiu et al., 2019, 2021). In this study, we further demonstrate that PIF4/HMR-mediated transcriptional regulation is achieved by recruiting the Mediator complex through their direct interactions with MED14 (Figure 5C).

The Mediator complex is required for virtually all Pol II-mediated transcription in eukaryotes (Jeronimo and Robert, 2017; Soutourina, 2018). As a crucial component of the Mediator complex, MED14 has long been known to play important roles in the transcription of key genes involved in various developmental processes and stress responses, including cell proliferation, shoot apical meristem development, trichome papillae development, salicylic acid-, methyl jasmonate-, and ethylene-mediated plant immune responses, abscisic acid-dependent drought responses, as well as cold and heat stress responses (Autran et al., 2002; Zhang et al.,

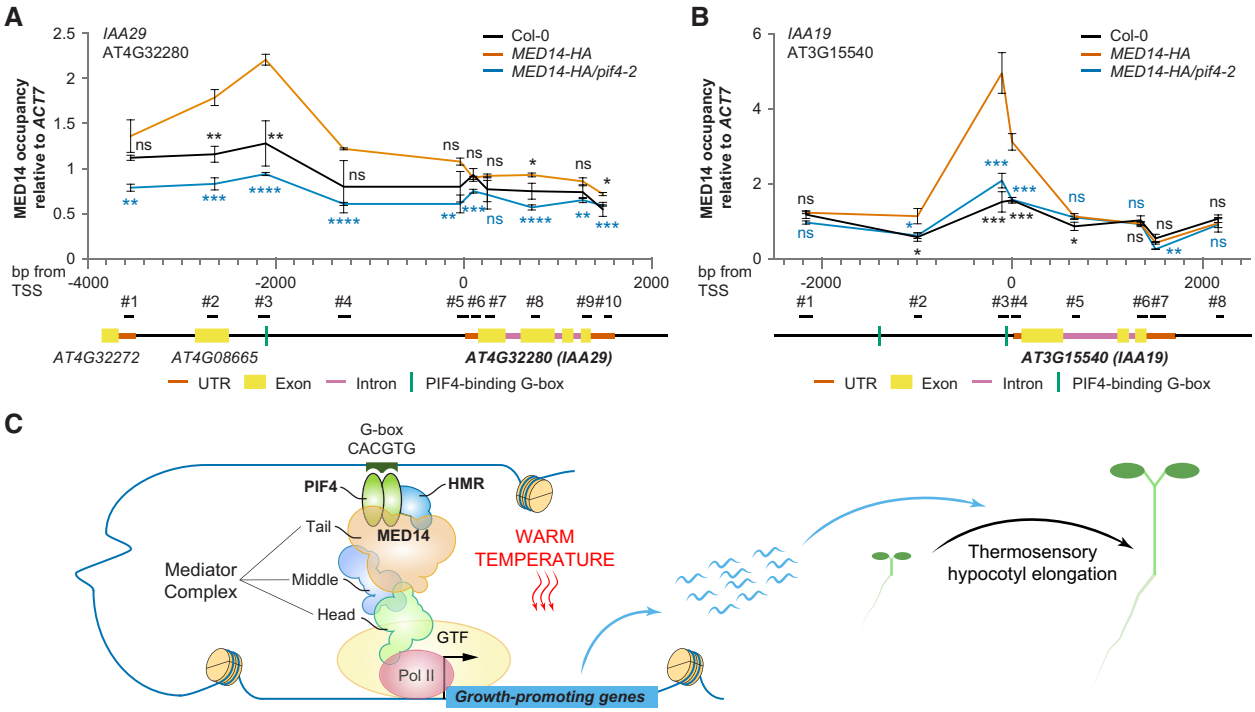

Figure 5 The association of MED14 with thermo-induced PIF4 direct targets is dependent on PIF4. ChIP-qPCR experiments compare MED14 occupancy across *IAA29* (A) or *IAA19* (B) in the presence and absence of PIF4. Col-0, *MED14–HA*, and *MED14–HA/pif4-2* were grown in continuous R light (50 μmol m^{-2} s^{-1}) at 20°C for 96 h and subsequently treated at 27°C in the same light condition for 6 h. HA antibodies were used to assay MED14–HA association with each gene. Values are mean ± SD from three independent samples, with data presented as the ratio of MED14–HA at *IAA*/input to MED14–HA at *ACT7* (+ 1912)/input. Student's *t* tests were used to compare the values between *MED14–HA* and other lines (n = 3; Col-0, black; *MED14–HA/pif4-2*, blue). $^{****}P < 0.0001$; $^{***}P < 0.001$; $^{**}P < 0.01$; $^{*}P < 0.05$; ns, not significant ($P \geq 0.05$). The exact position of each PCR fragment is shown in the illustrations at the bottom and the primers are listed in Supplemental Table S4. The transcription start site (TSS) is the first nucleotide of the 5′-untranslated region (UTR), as defined by the Araport11 genome annotation, released in June 2016. C, Schematic model for MED14 recruitment by PIF4 and HMR during the thermo-induced transcription of growth-promoting PIF4 target genes, the products of which subsequently promote thermosensory hypocotyl elongation. Pol II, RNA polymerase II; GTF, general transcription factors. The black arrow indicates the TSS. The size and proportions of the depicted components do not reflect their actual dimensions.

2013; Hemsley et al., 2014; Wang et al., 2016; Fornero et al., 2019; Ohama et al., 2020; Lee et al., 2021a). In particular, MED14 works with MED16 and MED2 in modulating cold-responsive genes regulated by the AP2 transcription factors C-repeat binding factors, and operates with MED17 in activating heat stress-inducible genes by assisting HsfA1, a heat shock transcription factor (HSF) that functions as a master regulator of the heat stress response (Hemsley et al., 2014; Ohama et al., 2020). We show here that MED14's function is not limited to plant responses to extreme cold or hot temperatures, rather, it is also indispensable for the transcription of growth-related genes involved in moderately elevated temperature responses (Figures 1–3).

Intriguingly, mutations in most Mediator head, middle, and kinase components did not affect thermosensory hypocotyl growth (Supplemental Figure S1). The only exception was *med17*, which showed markedly shorter hypocotyl at 27°C and reduced thermal response when compared with the wild-type seedlings. This result is consistent with a recent study showing that MED17 binds to and facilitates the enrichment of H3K4me3 on the promoters of thermosensory genes such as *PIF4*, *YUC8*, *IAA19*, and *IAA29* (Agrawal et al., 2022). Two mechanisms could potentially lead to the lack of phenotype in other Mediator mutants. First, it could be caused by functional redundancy. This may be the case for *med22a/med22b*, *med7a/med7b*, and *med10a/med10b* (Supplemental Figure S1) and could be tested with higher order mutants in future studies. Secondly, although the "relative response" phenotypes of some Mediator mutants were the same as the wild-type, the absolute hypocotyl length at both 20°C and 27°C was shorter than that of the wild-type (e.g. *med22a*, *med7a*, *cycCa*; Supplemental Figure S1). This suggests that some Mediator subunits are equally important for hypocotyl growth at both lower (20°C) and warmer temperatures (27°C), that is their roles in hypocotyl elongation are not temperature dependent. We also want to emphasize that some Mediator subunits (e.g. MED1, MED4, MED12, etc.) are essential for Arabidopsis growth and development and null mutants of these subunits are either embryonic or seedling lethal. We did not include these mutants in the current study but highlighted them in Supplemental Figure S1.

In higher eukaryotes, Mediator contains at least seven tail components, namely MED2/29/32, MED3/27, MED5/24/33,

MED15, MED16, MED23, and MED25 (Buendía-Monreal and Gillmor, 2016; Dolan and Chapple, 2017; Soutourina, 2018). Although originally assigned to the tail module (Dotson et al., 2000), MED14 was later found to play a more complex and critical role in both basal and activated transcription. For example, the cryo-electron microscopy (Cryo-EM) structure of *Schizosaccharomyces pombe* Mediator revealed that yeast MED14 functions as a backbone that connects the head, middle, and tail modules (Tsai et al., 2017). Likewise, *Mus musculus* MED14 is also centrally positioned, which enables inter-module interactions and makes it heavily involved in tail interactions (Zhao et al., 2021). Although it has not been definitively determined, Arabidopsis MED14 may possess similar structural features and play equally important roles in bridging all three modules as well as interacting with specific transcription factors, as suggested here by our data showing that MED14 physically interacts with activators PIF4 and HMR for thermoresponsive gene expression (Figure 4).

Nevertheless, the precise molecular details underlying the PIF4/HMR–MED14 interaction and the subsequent transcriptional activation of thermo-induced genes have yet to be revealed. Recent studies revealed that a variety of mammalian and yeast transcription factors form phase-separated condensates with Mediator through diverse TADs and that the formation of such condensates is associated with gene activation (Boija et al., 2018; Sabari et al., 2018). The phase-separating capacity of TADs and Mediator subunits is endowed by intrinsically disordered regions (IDRs), low-complexity protein segments that lack a defined secondary structure. In most eukaryotes, $>80\%$ of transcription factors and 75% of Mediator subunits possess extended ($\geqslant 30$ residues) IDRs (Liu et al., 2006; Tóth-Petróczy et al., 2008). Similarly, numerous plant transcription factors and Mediator subunits are predicted to contain at least one IDR (Nagulapalli et al., 2016; Salladini et al., 2020). In particular, the bHLH transcription factor family, to which PIF4 belongs, is hypothesized to have a general ability to undergo spontaneous liquid–liquid phase separation in transcription regulation by their IDRs (Tarczewska and Greb-Markiewicz, 2019; Salladini et al., 2020). Both PIF4 and HMR possess TADs that are potentially intrinsically disordered and thus could contribute to interactions with the Mediator complex. PIF4's TAD contains a variant of the ΦxxΦΦ motif (Φ indicates a bulky hydrophobic residue and x is any other amino acid) flanked by multiple acidic residues, a structural feature that resembles the activator motifs in other activators such as mammalian p53 and yeast Gcn4 (Yoo et al., 2021). Mutating the ΦxxΦΦ motif reduced PIF4 transcriptional activity in yeast (Yoo et al., 2021). HMR possesses an acidic-type 9aaTAD, the mutation of which drastically reduces its transactivation activity (Qiu et al., 2015) and affects MED14 recruitment to the promoter of PIF4-regulated thermo-induced genes (Supplemental Figure S8). However, mutating HMR's TAD exerts pleiotropic effects on transcriptional machinery in thermomorphogenesis. Both PIF4 protein accumulation and *MED14* transcript abundance at warm temperatures were dramatically reduced in the *hmr-22* background (Supplemental Figure S7, C–F), suggesting that HMR's TAD is required for the accumulation of the transcription activator and co-activator complex. On the other hand, it is still unclear whether HMR's TAD is directly involved in recruiting MED14 to the promoters of growth-promoting PIF4 target genes upon moderate temperature elevations. Future research will focus on unraveling the interaction mechanism between PIF4/HMR and MED14 upon temperature changes.

Besides its central role in thermomorphogenesis, PIF4 is also known for its function in shade avoidance (Lorrain et al., 2008; Hornitschek et al., 2009). A recent study reported that tomato PIF4 promotes shade-induced hypocotyl elongation by recruiting MED25 to regulate the expression of genes that encode auxin biosynthesis and auxin signaling proteins (Sun et al., 2020). Two *med25* loss-of-function mutants also showed reduced thermosensory hypocotyl growth (Figure 1, B and C), suggesting a potential function of MED25 in thermomorphogenesis and that multiple tail subunits may simultaneously contribute to the thermal response. We also tested whether MED14 is also involved in the shade-avoidance response. Like *pif4-2* and *hmr-22*, the *med14* mutant showed a severe defect in low R/FR ratio-mediated shade avoidance (Supplemental Figure S3). Therefore, it would be interesting to study the shared and unique mechanisms by which PIF4/HMR recruits Mediator tail subunits MED14 and MED25 in different signaling pathways triggered by two environmental cues.

Materials and methods

Plant materials and growth conditions

All the Arabidopsis (*Arabidopsis thaliana*) mutants used in this study are in the Col-0 background. Mediator mutants were obtained from the Arabidopsis Biological Resource Center and the detailed list is shown in Supplemental Table S1. Homozygosity was confirmed by polymerase chain reaction (PCR) before the seeds were used for phenotyping. Other Arabidopsis mutants, including *pif4-2* (SAIL_1288_E07) and *hmr-22*, were previously described (Leivar et al., 2008; Qiu et al., 2015, 2019). Seeds were briefly rinsed with 70% (v/v) ethanol and surface sterilized with bleach (3% sodium hypochlorite, w/v) for 10 min before being plated on half-strength Murashige and Skoog (1/2 MS) media supplemented with Gamborg's vitamins (MSP0506, Caisson Laboratories, North Logan, UT, USA), 0.5-mM MES (pH 5.7), and 0.8% (w/v) agar (A038, Caisson Laboratories, North Logan, UT, USA). Seeds were stratified in the dark at 4°C for 3–5 days to synchronize germination before treatment under specific light and temperature conditions in LED chambers (Percival Scientific, Perry, IA, USA). Unless otherwise stated, seedlings were grown in continuous R light (50 μmol m^{-2} s^{-1}). Fluence rates of light were measured using an Apogee PS200 spectroradiometer (Apogee Instruments Inc., Logan, UT, USA).

Seedling measurements

For quantification of hypocotyl length, petiole length, and petiole angles under continuous R light (50 μmol m^{-2} s^{-1}), seedlings were grown at either 20°C or 27°C for 96 h. For quantification of hypocotyl length under continuous white light (35 μmol m^{-2} s^{-1}), seedlings were grown at either 20°C (R/FR ratio = 10.2), 20°C (R/FR = 0.4), or 27°C (R/FR = 10.2) for 12 days. Seedlings from each line were placed on transparency film paper and scanned using an Epson Perfection V700 photo scanner. Hypocotyl length, petiole length, and petiole angles were measured using NIH ImageJ software (http://rsb.info.nih.gov/nih-image/). The percent increase in the hypocotyl/petiole length or petiole angle of each line was calculated as the percentage of the rise in hypocotyl/petiole length or petiole angle at 27°C compared with that at 20°C. The relative response (for hypocotyl or petiole length) of a mutant is defined as the percentage of its PI value or temperature response relative to that of Col-0. At least three replicates were used to calculate the mean and standard deviation of each relative response. Violin and box plots were generated using Prism 9 (GraphPad Software, San Diego, CA).

Plasmid constructions

All PCR reactions were performed using the Q5 High-Fidelity DNA Polymerase and the ligation reactions with the NEBuilder HiFi DNA Assembly Master Mix (New England Biolabs Inc., Ipswich, MA, USA). To generate the binary vector for making *MED14* transgenic lines, the full-length coding sequence (CDS) of *MED14* was fused with the sequence of a *$(PT)_4P$ linker* and three copies of an *HA-tag* when being cloned into the binary vector pCHF1 between SacI and BamHI. The bait vectors used in GST pull-down assays were either made previously (Qiu et al., 2015) or generated by cloning the full-length CDS of *PIF4* into pET42b vectors between BamHI and HindIII, and prey vectors were constructed by cloning the full-length CDS of *MED14* into the pCMX-PL2-NterHA vector between EcoRI and BamHI. Vectors used for the Bimolecular fluorescence complementation assay were generated by cloning the full-length CDS of *PIF4* and *HMR* into MCS I of pDOE-01 (ABRC stock# CD3-1901) between NcoI and SpeI, followed by cloning the full-length CDS of *MED14* into MCS III between KfiI and AatII. All the primers used for plasmid constructions are listed in Supplemental Table S2.

Generation of transgenic lines

To generate the *35S::MED14–HA/med14* transgenic lines, the *med14* mutant was transformed with the above-described *pCHF1-MED14-$(PT)_4$P-3 × HA* plasmid using the *Agrobacterium*-mediated floral dip method. The transformants were selected on the 1/2 MS medium containing 100 μg·mL^{-1} gentamycin. At least 10 independent lines that segregated approximately 3:1 for gentamycin resistance in the T2 generation were identified and two of these lines were selected for this study based on the transgene expression level. For all experiments, T3 self-progenies of homozygous T2 plants were used.

RNA extraction and RT–qPCR

Total RNA was extracted from 50 to 100 mg seedlings using the Quick-RNA Miniprep Kit with on-column DNase I digestion (Zymo Research, Irvine, CA, USA). cDNA was synthesized with 2–2.5 μg total RNA using the Invitrogen SuperScript III Reverse Transcriptase and the $Oligo(dT)_{20}$ primer (Thermo Fisher Scientific, Waltham, MA, USA). For RT–qPCR, cDNA diluted in nuclease-free water was mixed with FastStart Universal SYBR Green Master (MilliporeSigma, Burlington, MA, USA) and gene-specific primers (Supplemental Table S3). RT–qPCR reactions were performed in triplicate with a Qiagen Rotor-Gene Q 5Plex real-time cycler (Qiagen, Germantown, MD, USA). Transcript levels of each gene were calculated relative to that of *PP2A*. A standard curve was performed for each gene to determine the linear range, efficiency, and reproducibility of the qPCR assay. The final RT–qPCR results were calculated by the $2^{-\Delta\Delta Ct}$ method using at least two biological replicates. Bar charts were generated using Prism 9 (GraphPad Software, San Diego, CA, USA).

RNA-seq and data analysis

RNA was isolated as described above. The RNA concentration and purity were determined spectrophotometrically using the Nanodrop 2000 instrument (Thermo Fisher Scientific, Waltham, MA), and assessing the continuous spectrum (190–840 nm) generated by the instrument for each sample. The quality of the RNA samples was evaluated on the Agilent 2100 Bioanalyzer (Agilent Technologies Inc., Santa Clara, CA, USA).

Sequencing libraries were generated with 300 ng to 1 μg of RNA using the TruSeq Stranded mRNA Sample Preparation Kit (Illumina, San Diego, CA, USA). The libraries were assessed for size and purity using the Agilent 2100 Bioanalyzer and quantitated by RT–qPCR using a KAPA Biosystems Library Quantitation kit (Roche, Pleasanton, CA, USA). Libraries were normalized, pooled, and diluted to a loading concentration of 1.8 pM, loaded on an Illumina High-Output Flow Cell, and sequenced on the Illumina NextSeq 500 instrument. The sequencing run generated ~16 million 150-bp paired-end reads per sample, and all run metrics, including Q-Score distributions, cluster densities, and total sequence yields, were within the recommended parameters.

Data analysis was performed using the Qiagen CLC Genomics Workbench (CLCGWB) version 21 software. The reads were mapped to the A. thaliana reference genome (TAIR10/Araport11 genome release), using default parameters with a strand-specific alignment protocol. The mapping report indicated that all metrics fell within the recommended parameters, with >90% of the reads per sample mapping to the reference genome. The mapping results generated values for Total Counts, Transcripts per Million reads, as well as FPKM for each gene. The "Differential Expression

for RNA-Seq" tool in CLCGWB software was used, with default parameters, to identify differentially expressed genes across samples. Genes that had a fold-change of $\geqslant 2$, an FDR-corrected $P < 0.001$, and a Maximum Group Mean FPKM of > 1 (i.e. the maximum of the average FPKM across the two groups in each statistical comparison) were considered to be significantly differentially expressed. The list of differentially expressed genes obtained in each statistical comparison is shown in Supplemental Data Set 1. Venn diagrams were generated using the Bioinformatics and Evolutionary Genomics website (https://bioinformatics.psb.ugent.be/webtools/Venn/). Hierarchical cluster analysis was performed with the Morpheus software tool available on the Broad Institute website (https://software.broadinstitute.org/morpheus/). Gene Ontology (GO) enrichment analyses were performed using the PANTHER classification tool available at the TAIR website (https://www.arabidopsis.org/tools/go_term_enrichment.jsp) or the GeneCodis 4 program (https://genecodis.genyo.es/; García-Moreno et al., 2022). For comparison of data with published datasets, the appropriate FastQ files available in the National Center for Biotechnology Information-Gene Expression Omnibus (NCBI-GEO) database were imported into CLCGWB software, and all analyses were conducted similarly to those described above. For the published datasets that utilized a 3′-TagSeq protocol, mapping was performed using the 3′-Sequencing option in the CLCGWB alignment parameters.

RNA-seq data accession number. The RNA-seq analysis data described in this article are accessible through accession no. GSE196969 at NCBI's Gene Expression Omnibus database.

Protein extraction and immunoblots

For immunoblots, total protein was extracted from 4-day-old seedlings as previously described (Qiu et al., 2019, 2021). Briefly, 200-mg seedlings were freshly homogenized using a BeadBug microtube homogenizer (Benchmark Scientific Inc., Sayreville, NJ, USA) in three volumes ($mg \cdot \mu L^{-1}$) of extraction buffer containing 100-mM Tris–HCl, pH 7.5, 100-mM NaCl, 5-mM EDTA, 5% (w/v) SDS, 20% (v/v) glycerol, 20-mM DTT, 40-mM β-mercaptoethanol, 2-mM phenylmethylsulfonyl fluoride, 40-μM MG115 (Apexbio Technology LLC, Houston, TX, USA), 40-μM MG132 (Cayman Chemical, Ann Arbor, MI, USA), 40-μM bortezomib (MilliporeSigma, Burlington, MA, USA), 10-mM N-ethylmaleimide (Thermo Fisher Scientific, Waltham, MA, USA), 1× phosphatase inhibitor cocktail 2 (Thermo Fisher Scientific, Waltham, MA, USA), 1× phosphatase inhibitor cocktail 3 (MilliporeSigma, Burlington, MA, USA), 1× EDTA-free protease inhibitor cocktail (MilliporeSigma, Burlington, MA, USA), and 0.01% (w/v) bromophenol blue. Samples were boiled for 10 min and centrifuged at 16,000*g* for 10 min. The supernatant was immediately used for immunoblots or stored at −80°C until use.

For immunoblots, cleared protein samples were separated via sodium dodecyl sulphate–polyacrylamide gel electrophoresis (SDS–PAGE), transferred to nitrocellulose membranes, probed with the indicated primary antibodies, and then incubated with 1:5,000 dilution of horseradish peroxidase-conjugated goat anti-rabbit or anti-mouse secondary antibodies (Bio-Rad Laboratories, 1706515 for anti-rabbit and 1706516 for anti-mouse). Primary antibodies, including monoclonal mouse anti-HA antibodies (MilliporeSigma, H3663), polyclonal rabbit anti-HMR antibodies (Chen et al., 2010), polyclonal goat anti-PIF4 antibodies (Agrisera, AS16 3955), and polyclonal rabbit anti-RPN6 antibodies (Enzo Life Sciences, BMLPW8370-0100) were used at 1:1,000 dilution. Signals were detected via chemiluminescence using a SuperSignal kit (Thermo Fisher Scientific, Waltham, MA, USA) and an Azure C600 Advanced Imaging System (Azure Biosystems, Dublin, CA, USA). To compare the protein levels (e.g. HMR and PIF4 in Figure 2C) among different genotypes, they were first normalized against the RPN6 protein level in the same sample, and then the relative protein level was calculated by comparing the normalized value with that in the control genotype (e.g. Col-0 before thermal treatment in Figure 2C), which was set to 1.

Chromatin immunoprecipitation

ChIP assays were performed as previously described with modifications (Wu et al., 2016). Seedlings grown on 1/2 MS medium in continuous R light (50 $\mu mol\ m^{-2}\ s^{-1}$) at 20°C for 96 h were treated at 27°C for 6 h before collecting. About 200-mg seedlings were cross-linked with 1% formaldehyde in 1× phosphate buffered saline (PBS) for 2 × 15 min by vacuum infiltration, followed by the addition of glycine to 125 mM with another 10 min of vacuum infiltration. Fixed seedlings were dried on a stack of paper towels after being washed with 4 × 10 mL cold PBS. Samples were ground into a fine powder in liquid nitrogen and resuspended in nuclear isolation buffer containing 20-mM Hepes, pH 7.6, 0.25-M sucrose, 5-mM KCl, 10-mM $MgCl_2$, 40% (v/v) glycerol, 0.25% (v/v) Triton X-100, 0.1-mM PMSF, 0.1% (v/v) β-mercaptoethanol, 1× complete EDTA-free protease inhibitor cocktail (MilliporeSigma, Burlington, MA, USA). Nuclei were enriched by filtering the lysate through two layers of Miracloth and centrifugation at 3,000*g* for 10 min at 4°C. Nuclear pellets were resuspended in nuclei lysis buffer (20-mM Tris–HCl, pH 7.5, 100-mM NaCl, 2.5-mM EDTA, 10% (v/v) glycerol, 1% (v/v) Triton X-100, 1× protease inhibitor cocktail) and sonicated with 25 cycles of 30-s-long pulses (30-s intervals) using a Bioruptor Plus (Diagenode, Denville, NJ, USA). Nuclear lysates were cleared with two rounds of centrifugation at 13,000*g* for 5 min at 4°C. Immunoprecipitation was performed by incubating 30 μL of Dynabeads Protein G (Thermo Fisher Scientific, Waltham, MA, USA), 2.5 μg of anti-HA tag antibody (Abcam, Waltham, MA, USA), and 1 mL of diluted chromatin (containing 100 μL of sonicated chromatin) at 4°C for 4 h. Beads were washed for 2 × 15 min with low-salt wash buffer (20-mM Tris–HCl, pH 7.5, 150-mM NaCl, 2.5-mM EDTA, 0.05% (w/v) SDS, 1% (v/v) Triton X-100), for 2 × 15 min with high-salt wash buffer (20-mM Tris–HCl, pH 7.5, 500-mM NaCl, 2.5-mM EDTA, 0.05% (w/v) SDS, 1% (v/v) Triton X-

100), for 1 × 15 min with LiCl Wash Buffer (20-mM Tris–HCl, pH 7.5, 250-mM LiCl, 1-mM EDTA, 0.5% (w/v) Na-deoxycholate, 0.5% (v/v) Nonidet P-40), and for 1 × 15 min with TE buffer (10-mM Tris–HCl, pH 7.5, 1-mM EDTA). Ten percent (w/v) chelex resin (Bio-Rad, Hercules, CA, USA) was mixed with the beads and immunoprecipitated DNA was eluted after reverse cross-linking by boiling at 95°C for 10 min, followed by treatment with 40 μg of proteinase K for 1 h at 55°C. Eluted DNA was recovered using the ChIP DNA Clean & Concentrator kit (Zymo Research, Irvine, CA, USA) and used for qPCR reactions. Primers for ChIP-qPCR are listed in Supplemental Table S4. Values are means ± SD from two independent samples; data are presented as a ratio of (MED14–HA *IAA*/input *IAA*) to (MED14–HA at internal control/input at internal control) to correct for tube-to-tube variation (the MED14–HA level at position +1912 in *Actin7* was used as an internal control for normalization).

GST pull-down

GST pull-down assays were performed as described previously (Qiu et al., 2015, 2021). The pET42b/PIF4 and pET42b/HMR vectors were constructed as described above and expressed as GST-PIF4 and GST-HMR fusion proteins in the *E. coli* strain BL21-CodonPlus (DE3) (Agilent Technologies). The pCMX-PL2-NterHA/MED14 vector was constructed as described above and expressed as HA-MED14 proteins using the TNT T7 Coupled Reticulocyte Lysate System (Promega, Madison, WI, USA). HA-MED14 prey proteins were incubated with the affinity-purified GST-PIF4 or GST-HMR bait proteins immobilized on glutathione Sepharose 4B beads (GE Healthcare, Chicago, IL, USA) at 4°C for 2 h. Beads were washed four times with E buffer (50-mM Tris–HCl, pH 7.5, 100-mM NaCl, 1-mM EDTA, 1-mM EGTA, 1% (v/v) dimethyl sulfoxide (DMSO), 2-mM DTT, 0.1% (v/v) Nonidet P-40). Bound proteins were eluted by boiling in 2× SDS loading buffer and used in subsequent SDS–PAGE and immunoblotting. Input and immunoprecipitated HA-MED14 prey proteins were detected using goat anti-HA polyclonal antibodies (GenScript, Piscataway, NJ, USA). The amounts of GST-PIF4 and GST-HMR bait proteins were visualized by staining the SDS–PAGE with Coomassie Brilliant Blue.

Agroinfiltration-based BiFC

The pDOE-01/PIF4 and pDOE-01/PIF4/MED14 vectors were constructed as shown above. The BiFC assays were performed as described (Gookin and Assmann, 2014). The constructed pDOE-01 vectors were transformed into GV3101 *Agrobacterium* electrocompetent cells and selected on 25-μg mL^{-1} rifampicin, 20-μg·mL^{-1} gentamycin, and 50-μg·mL^{-1} kanamycin at 29°C for 2–3 days. Several colonies of positive transformants were harvested from the plate, inoculated to LB media containing the above-mentioned antibiotics, and cultured at 29°C for 2 h with 100-μM acetosyringone (MilliporeSigma, Burlington, MA, USA). *Agrobacterium* cells were washed with and diluted to an OD_{600} of 0.1 in the infiltration buffer (10-mM MES-KOH, pH 5.6, 10-mM $MgCl_2$, and 100-μM acetosyringone). *Agrobacterium* cells containing the pCHF3/CFP plasmid were treated in the same way and mixed with those containing the pDOE-01 vectors for co-infiltration.

Nicotiana benthamiana plants were grown in General Purpose Pro-Mix BX (Premier Tech Horticulture, Quakertown, PA, USA) in a growth room with 150-μmol·m^{-2}·s^{-1} white light, 14-h light/10-h dark cycles, and a temperature range between 21°C and 24°C. BiFC control and test infiltrations were performed on three plants each. Fluorescence signals were examined 40–70 h after agroinfiltration using a Leica SP8 Inverted Confocal Microscope (Leica Microsystems Inc., Buffalo Grove, IL, USA). The laser output power and intensity were set to 70% and 10%, respectively. The mVenus signal was excited with a white light laser at 488 nm and emissions were captured at 500–550 nm with a gain of 456. The CFP signal was excited using a 408-nm diode laser and emissions were captured at 460–490 nm with a gain of 362. All the signals were co-detected with chlorophyll autofluorescence, which was captured at 650–700 nm with a gain of 437.

Accession numbers

Accession numbers are as described by TAIR (https://www.arabidopsis.org) as follows: PHYTOCHROME-INTERACTING FACTOR 4 (PIF4), AT2G43010; HEMERA (HMR), AT2G34640; MED2/29/32, AT1G11760; MED3/27, AT3G09180; MED5A/33A, AT3G23590; MED5B/33B, AT2G48110; MED6, AT3G21350; MED7A, AT5G03220; MED7B, AT5G03500; MED8, AT2G03070; MED9, AT1G55080; MED10A, AT5G41910; MED10B, AT1G26665; MED14, AT3G04740; MED16, AT4G04920; MED17, AT5G20170; MED18, AT2G22370; MED19A, AT5G12230; MED22A, AT1G16430; MED22B, AT1G07950; MED23, AT1G23230; MED25, AT1G25540; MED28, AT3G52860; MED30, AT5G63480; MED31, AT5G19910; CYCLIN C1-2 (CYCCA), AT5G48630; CYCLIN C1-1 (CYCCB), AT5G48640; SERINE/THREONINE PROTEIN PHOSPHATASE 2A (PP2A), AT1G13320; YUCCA8 (YUC8), AT4G28720; INDOLE-3-ACETIC ACID INDUCIBLE 19 (IAA19), AT3G15540; INDOLE-3-ACETIC ACID INDUCIBLE 29 (IAA29), AT4G32280; SULFOTRANSFERASE 2A (ST2A), AT5G07010; ARABIDOPSIS PP2C CLADE D 7 (APD7), AT5G02760; AUXIN-REGULATED GENE INVOLVED IN ORGAN SIZE (ARGOS), AT3G59900; RING, AT1G24580; SERINE CARBOXYPEPTIDASE-LIKE 31 (SCPL31), AT1G11080; METHYL ESTERASE 18 (MES18), AT5G58310; ACTIN 7 (ACT7), AT5G09810.

Supplemental data

The following materials are available in the online version of this article.

Supplemental Figure S1. Thermomorphogenetic hypocotyl responses in mediator mutants.

Supplemental Figure S2. MED14 regulates warm temperature-induced petiole elongation and leaf hyponastic response.

Supplemental Figure S3. MED14 is required for both warm temperature- and shade-induced hypocotyl elongation.

Supplemental Figure S4. Quantification of HMR and PIF4 protein levels during thermal treatments.

Supplemental Figure S5. Comparison of thermoresponsive transcriptomes in different studies.

Supplemental Figure S6. Analysis of PIF4/HMR/MED14-dependent thermoresponsive genes.

Supplemental Figure S7. Characterization of *35S::MED14–HA* lines crossed with *pif4-2* and *hmr-22*.

Supplemental Figure S8. The association of MED14 with thermo-induced PIF4 direct targets is reduced in the *hmr-22* mutant.

Supplemental Table S1. List of T-DNA insertion lines and genotyping primers used in this study.

Supplemental Table S2. Primers used for plasmid construction.

Supplemental Table S3. RT–qPCR primers for the genes examined in this study.

Supplemental Table S4. ChIP-qPCR primers for the genes examined in this study.

Supplemental Data Set S1. Lists of SSTF genes regulated by warm temperatures in Col-0, *pif4-2*, *hmr-22*, and *med14*.

Supplemental Data Set S2. Lists of thermo-responsive genes in two other reports.

Supplemental Data Set S3. Lists of PIF4/HMR/MED14-dependent thermo-responsive genes.

Supplemental Data Set S4. Lists of potential PIF4/HMR/MED14-dependent, thermo-responsive PIF4 direct targets.

Data availability statement

The original contributions presented in the study are included in the article/Supplementary Material, further inquiries can be directed to the corresponding author. The datasets presented in this study can be found in online repositories. The names of the repository/repositories and accession number(s) can be found in NCBI's Gene Expression Omnibus database (https://www.ncbi.nlm.nih.gov/geo/), GSE196969.

Acknowledgments

We would like to thank Dr. Gregg Roman and Dr. Ruofan Cao in the Imaging Research Core of GlyCORE at the University of Mississippi for their assistance with the usage of the Leica SP8 Inverted Confocal Microscope. We also thank all the lab members, especially Ranjeeta Odari and Anupa Wasti, for their critical comments and suggestions regarding the manuscript.

Funding

This work was supported by a grant from the National Science Foundation (NSF) (IOS-2200200) and startup funds from the University of Mississippi (Oxford, MS) to Y.Q. The early stages of these studies were performed in Meng Chen laboratory at the University of California at Riverside, with funding from the National Institute of General Medical Sciences (NIGMS) of the National Institutes of Health (NIH) (R01GM087388) to M.C. The work related to the confocal microscope was supported by an Institutional Development Award (IDeA) from NIGMS of the NIH under award number P20GM103460 to the Imaging Research Core of the Glycoscience Center of Research Excellence (GlyCORE) at the University of Mississippi.

Conflict of interest statement. The authors have no conflict of interest to declare.

References

Agrawal R, Sharma M, Dwivedi N, Maji S, Thakur P, Junaid A, Fajkus J, Laxmi A, Thakur JK (2022) MEDIATOR SUBUNIT17 integrates jasmonate and auxin signaling pathways to regulate thermomorphogenesis. Plant Physiol **189**: 2259–2280

Autran D, Jonak C, Belcram K, Beemster GTS, Kronenberger J, Grandjean O, Inzé D, Traas J (2002) Cell numbers and leaf development in Arabidopsis: a functional analysis of the STRUWWELPETER gene. EMBO J **21**: 6036–6049

Boija A, Klein IA, Sabari BR, Dall'Agnese A, Coffey EL, Zamudio AV, Li CH, Shrinivas K, Manteiga JC, Hannett NM, et al. (2018) Transcription factors activate genes through the phase-separation capacity of their activation domains. Cell **175**: 1842–1855.e16

Bordiya Y, Kim J, Xi Y, Kim D-H, Pyo Y, Zhao B, Zong W, Ricci WA, Zhang X, Sung S (2020) VIL1, a Polycomb-associated protein, modulates high ambient temperature response via H3K27me3 and H2A.Z in Arabidopsis thaliana. bioRxiv 2020.04.29.069484; doi: https://doi.org/10.1101/2020.04.29.069484

Borggrefe T, Yue X (2011) Interactions between subunits of the Mediator complex with gene-specific transcription factors. Semin Cell Dev Biol **22**: 759–768

Bourbon H-M (2008) Comparative genomics supports a deep evolutionary origin for the large, four-module transcriptional mediator complex. Nucleic Acids Res **36**: 3993–4008

Box MS, Huang BE, Domijan M, Jaeger KE, Khattak AK, Yoo SJ, Sedivy EL, Jones DM, Hearn TJ, Webb AAR, et al. (2015) ELF3 controls thermoresponsive growth in Arabidopsis. Curr Biol **25**: 194–199

Buendía-Monreal M, Gillmor CS (2016) Mediator: a key regulator of plant development. Dev Biol **419**: 7–18

Casal JJ, Balasubramanian S (2019) Thermomorphogenesis. Annu Rev Plant Biol **70**: 321–346

Cevher MA, Shi Y, Li D, Chait BT, Malik S, Roeder RG (2014) Reconstitution of active human core Mediator complex reveals a critical role of the MED14 subunit. Nat Struct Mol Biol **21**: 1028–1034

Chen M, Galvão RM, Li M, Burger B, Bugea J, Bolado J, Chory J (2010) Arabidopsis HEMERA/pTAC12 initiates photomorphogenesis by phytochromes. Cell **141**: 1230–1240

Chen X, Yin X, Li J, Wu Z, Qi Y, Wang X, Liu W, Xu Y (2021) Structures of the human Mediator and Mediator-bound preinitiation complex. Science **372**: eabg0635

Cortijo S, Charoensawan V, Brestovitsky A, Buning R, Ravarani C, Rhodes D, van Noort J, Jaeger KE, Wigge PA (2017) Transcriptional regulation of the ambient temperature response by H2A.Z nucleosomes and HSF1 transcription factors in Arabidopsis. Mol Plant **10**: 1258–1273

Dalton JC, Bätz U, Liu J, Curie GL, Quail PH (2016) A modified reverse one-hybrid screen identifies transcriptional activation domains in PHYTOCHROME-INTERACTING FACTOR 3. Front Plant Sci **7**: 881

Ding L, Wang S, Song Z-T, Jiang Y, Han J-J, Lu S-J, Li L, Liu J-X (2018) Two B-box domain proteins, BBX18 and BBX23, interact with ELF3 and regulate thermomorphogenesis in Arabidopsis. Cell Rep **25**: 1718–1728.e4

Dolan WL, Chapple C (2017) Conservation and divergence of mediator structure and function: insights from plants. Plant Cell Physiol **58**: 4–21

Dolan WL, Dilkes BP, Stout JM, Bonawitz ND, Chapple C (2017) Mediator complex subunits MED2, MED5, MED16, and MED23 genetically interact in the regulation of phenylpropanoid biosynthesis. Plant Cell **29**: 3269–3285

Dotson MR, Yuan CX, Roeder RG, Myers LC, Gustafsson CM, Jiang YW, Li Y, Kornberg RD, Asturias FJ (2000) Structural organization of yeast and mammalian mediator complexes. Proc Natl Acad Sci USA **97**: 14307–14310

Fornero C, Rickerd T, Kirik V (2019) Papillae formation on Arabidopsis leaf trichomes requires the function of Mediator tail subunits 2, 14, 15a, 16, and 25. Planta **249**: 1063–1071

Franklin KA, Lee SH, Patel D, Kumar SV, Spartz AK, Gu C, Ye S, Yu P, Breen G, Cohen JD, et al. (2011) Phytochrome-interacting factor 4 (PIF4) regulates auxin biosynthesis at high temperature. Proc Natl Acad Sci USA **108**: 20231–20235

García-Moreno A, López-Domínguez R, Villatoro-García JA, Ramirez-Mena A, Aparicio-Puerta E, Hackenberg M, Pascual-Montano A, Carmona-Saez P (2022) Functional Enrichment Analysis of Regulatory Elements. Biomedicines **10**: 590

Gookin TE, Assmann SM (2014) Significant reduction of BiFC non-specific assembly facilitates in planta assessment of heterotrimeric G-protein interactors. Plant J **80**: 553–567

Han X, Yu H, Yuan R, Yang Y, An F, Qin G (2019) Arabidopsis transcription factor TCP5 controls plant thermomorphogenesis by positively regulating PIF4 activity. iScience **15**: 611–622

Hemsley PA, Hurst CH, Kaliyadasa E, Lamb R, Knight MR, De Cothi EA, Steele JF, Knight H (2014) The Arabidopsis mediator complex subunits MED16, MED14, and MED2 regulate mediator and RNA polymerase II recruitment to CBF-responsive cold-regulated genes. Plant Cell **26**: 465–484

Hornitschek P, Lorrain S, Zoete V, Michielin O (2009) Inhibition of the shade avoidance response by formation of non-DNA binding bHLH heterodimers. EMBO J **28**: 3893–3902

Jeronimo C, Robert F (2017) The Mediator complex: at the nexus of RNA polymerase II transcription. Trends Cell Biol **27**: 765–783

Jin H, Lin J, Zhu Z (2020) PIF4 and HOOKLESS1 impinge on common transcriptome and isoform regulation in thermomorphogenesis. Plant Commun **1**: 100034

Kim S, Hwang G, Kim S, Thi TN, Kim H, Jeong J, Kim J, Kim J, Choi G, Oh E (2020) The epidermis coordinates thermoresponsive growth through the phyB-PIF4-auxin pathway. Nat Commun **11**: 1053

Koini MA, Alvey L, Allen T, Tilley CA, Harberd NP, Whitelam GC, Franklin KA (2009) High temperature-mediated adaptations in plant architecture require the bHLH transcription factor PIF4. Curr Biol **19**: 408–413

Kumar SV, Lucyshyn D, Jaeger KE, Alós E, Alvey E, Harberd NP, Wigge PA (2012) Transcription factor PIF4 controls the thermosensory activation of flowering. Nature **484**: 242–245

Lee M, Dominguez-Ferreras A, Kaliyadasa E, Huang W-J, Antony E, Stevenson T, Lehmann S, Schäfer P, Knight MR, Ntoukakis V, et al. (2021a) Mediator subunits MED16, MED14, and MED2 are required for activation of ABRE-dependent transcription in Arabidopsis. Front Plant Sci **12**: 649720

Lee S, Paik I, Huq E (2020) SPAs promote thermomorphogenesis by regulating the phyB-PIF4 module in Arabidopsis. Development **147**: dev189233

Lee S, Wang W, Huq E (2021b) Spatial regulation of thermomorphogenesis by HY5 and PIF4 in Arabidopsis. Nat Commun **12**: 3656

Lee S, Zhu L, Huq E (2021c) An autoregulatory negative feedback loop controls thermomorphogenesis in Arabidopsis. PLoS Genet **17**: e1009595

Leivar P, Monte E (2014) PIFs: systems integrators in plant development. Plant Cell **26**: 56–78

Leivar P, Monte E, Oka Y, Liu T, Carle C, Castillon A, Huq E, Quail PH (2008) Multiple phytochrome-interacting bHLH transcription factors repress premature seedling photomorphogenesis in darkness. Curr Biol **18**: 1815–1823

Leivar P, Quail PH (2011) PIFs: pivotal components in a cellular signaling hub. Trends Plant Sci **16**: 19–28

Liu H-C, Charng Y-Y (2013) Common and distinct functions of Arabidopsis class A1 and A2 heat shock factors in diverse abiotic stress responses and development. Plant Physiol **163**: 276–290

Liu J, Perumal NB, Oldfield CJ, Su EW, Uversky VN, Dunker AK (2006) Intrinsic disorder in transcription factors. Biochemistry **45**: 6873–6888

Lorrain S, Allen T, Duek PD, Whitelam GC, Fankhauser C (2008) Phytochrome-mediated inhibition of shade avoidance involves degradation of growth-promoting bHLH transcription factors. Plant J **53**: 312–323

Ludwig W, Hayes S, Trenner J, Delker C, Quint M (2021) On the evolution of plant thermomorphogenesis. J Exp Bot **72**: 7345–7358

Ma D, Li X, Guo Y, Chu J, Fang S, Yan C, Noel JP, Liu H (2016) Cryptochrome 1 interacts with PIF4 to regulate high temperature-mediated hypocotyl elongation in response to blue light. Proc Natl Acad Sci USA **113**: 224–229

Maji S, Dahiya P, Waseem M, Dwivedi N, Bhat DS, Dar TH, Thakur JK (2019) Interaction map of Arabidopsis Mediator complex expounding its topology. Nucleic Acids Res **47**: 3904–3920

Malik S, Roeder RG (2010) The metazoan Mediator co-activator complex as an integrative hub for transcriptional regulation. Nat Rev Genet **11**: 761–772

Nagulapalli M, Maji S, Dwivedi N, Dahiya P, Thakur JK (2016) Evolution of disorder in Mediator complex and its functional relevance. Nucleic Acids Res **44**: 1591–1612

Nevarez PA, Qiu Y, Inoue H, Yoo CY, Benfey PN, Schnell DJ, Chen M (2017) Mechanism of dual targeting of the phytochrome signaling component HEMERA/pTAC12 to plastids and the nucleus. Plant Physiol **173**: 1953–1966

Nozawa K, Schneider TR, Cramer P (2017) Core Mediator structure at 3.4 Å extends model of transcription initiation complex. Nature **545**: 248–251

Ohama N, Moo TL, Chua N-H (2020) Differential requirement of MED14/17 recruitment for activation of heat inducible genes. New Phytol **229**: 3360–3376

Oh E, Zhu JY, Wang ZY (2012) Interaction between BZR1 and PIF4 integrates brassinosteroid and environmental responses. Nat Cell Biol **14**: 802–809

Park Y-J, Kim JY, Lee J-H, Han S-H, Park C-M (2021) External and internal reshaping of plant thermomorphogenesis. Trends Plant Sci **26**: 810–821

Park Y-J, Lee H-J, Ha J-H, Kim JY, Park C-M (2017) COP1 conveys warm temperature information to hypocotyl thermomorphogenesis. New Phytol **215**: 269–280

Pedmale UV, Huang S-SC, Zander M, Cole BJ, Hetzel J, Ljung K, Reis PAB, Sridevi P, Nito K, Nery JR, et al. (2016) Cryptochromes interact directly with PIFs to control plant growth in limiting blue light. Cell **164**: 233–245

Pfeiffer A, Shi H, Tepperman JM, Zhang Y, Quail PH (2014) Combinatorial complexity in a transcriptionally centered signaling hub in Arabidopsis. Mol Plant **7**: 1598–1618

Pham VN, Kathare PK, Huq E (2018) Phytochromes and phytochrome interacting factors. Plant Physiol **176**: 1025–1038

Piskacek S, Gregor M, Nemethova M, Grabner M, Kovarik P, Piskacek M (2007) Nine-amino-acid transactivation domain: establishment and prediction utilities. Genomics **89**: 756–768

Qiu Y (2020) Regulation of PIF4-mediated thermosensory growth. Plant Sci **297**: 110541

Qiu Y, Li M, Kim RJ-A, Moore CM, Chen M (2019) Daytime temperature is sensed by phytochrome B in Arabidopsis through a transcriptional activator HEMERA. Nat Commun **10**: 140

Qiu Y, Li M, Pasoreck EK, Long L, Shi Y, Galvão RM, Chou CL, Wang H, Sun AY, Zhang YC, et al. (2015) HEMERA couples the proteolysis and transcriptional activity of PHYTOCHROME INTERACTING FACTORs in Arabidopsis photomorphogenesis. Plant Cell **27**: 1409–1427

Qiu Y, Pasoreck EK, Yoo CY, He J, Wang H, Bajracharya A, Li M, Larsen HD, Cheung S, Chen M (2021) RCB initiates Arabidopsis thermomorphogenesis by stabilizing the thermoregulator PIF4 in the daytime. Nat Commun **12**: 2042

Rengachari S, Schilbach S, Aibara S, Dienemann C (2021) Structure of the human Mediator–RNA polymerase II pre-initiation complex. Nature **594**: 129–133

Robinson PJ, Trnka MJ, Bushnell DA, Davis RE, Mattei P-J, Burlingame AL, Kornberg RD (2016) Structure of a complete Mediator-RNA polymerase II pre-initiation complex. Cell **166**: 1411–1422.e16

Robinson PJ, Trnka MJ, Pellarin R, Greenberg CH, Bushnell DA, Davis R, Burlingame AL, Sali A, Kornberg RD (2015) Molecular architecture of the yeast Mediator complex. eLife **4**: e08719

Sabari BR, Dall'Agnese A, Boija A, Klein IA, Coffey EL, Shrinivas K, Abraham BJ, Hannett NM, Zamudio AV, Manteiga JC, et al. (2018) Coactivator condensation at super-enhancers links phase separation and gene control. Science **361**: eaar3958

Salladini E, Jørgensen MLM, Theisen FF, Skriver K (2020) Intrinsic disorder in plant transcription factor systems: functional implications. Int J Mol Sci **21**: 9755

Schilbach S, Hantsche M, Tegunov D, Dienemann C, Wigge C, Urlaub H, Cramer P (2017) Structures of transcription pre-initiation complex with TFIIH and Mediator. Nature **551**: 204–209

Sidaway-Lee K, Costa MJ, Rand DA, Finkenstadt B, Penfield S (2014) Direct measurement of transcription rates reveals multiple mechanisms for configuration of the Arabidopsis ambient temperature response. Genome Biol **15**: R45

Soutourina J (2018) Transcription regulation by the Mediator complex. Nat Rev Mol Cell Biol **19**: 262–274

Stavang JA, Gallego-Bartolomé J, Gómez MD, Yoshida S, Asami T, Olsen JE, García-Martínez JL, Alabadí D, Blázquez MA (2009) Hormonal regulation of temperature-induced growth in Arabidopsis. Plant J **60**: 589–601

Sun J, Qi L, Li Y, Chu J, Li C (2012) PIF4-mediated activation of YUCCA8 expression integrates temperature into the auxin pathway in regulating Arabidopsis hypocotyl growth. PLoS Genet **8**: e1002594

Sun W, Han H, Deng L, Sun C, Xu Y, Lin L, Ren P, Zhao J, Zhai Q, Li C (2020) Mediator subunit MED25 physically interacts with PHYTOCHROME INTERACTING FACTOR4 to regulate shade-induced hypocotyl elongation in tomato. Plant Physiol **184**: 1549–1562

Tarczewska A, Greb-Markiewicz B (2019) The significance of the intrinsically disordered regions for the functions of the bHLH transcription factors. Int J Mol Sci **20**: 5306

Tóth-Petróczy A, Oldfield CJ, Simon I, Takagi Y, Dunker AK, Uversky VN, Fuxreiter M (2008) Malleable machines in transcription regulation: the mediator complex. PLoS Comput Biol **4**: e1000243

Tsai K-L, Tomomori-Sato C, Sato S, Conaway RC, Conaway JW, Asturias FJ (2014) Subunit architecture and functional modular rearrangements of the transcriptional mediator complex. Cell **158**: 463

Tsai K-L, Yu X, Gopalan S, Chao T-C, Zhang Y, Florens L, Washburn MP, Murakami K, Conaway RC, Conaway JW, et al. (2017) Mediator structure and rearrangements required for holoenzyme formation. Nature **544**: 196–201

Vojnic E, Mourão A, Seizl M, Simon B, Wenzeck L, Larivière L, Baumli S, Baumgart K, Meisterernst M, Sattler M, et al. (2011) Structure and VP16 binding of the Mediator Med25 activator interaction domain. Nat Struct Mol Biol **18**: 404–409

Wang C, Du X, Mou Z (2016) The Mediator complex subunits MED14, MED15, and MED16 are involved in defense signaling crosstalk in Arabidopsis. Front Plant Sci **7**: 1947

Wu Z, Ietswaart R, Liu F, Yang H, Howard M, Dean C (2016) Quantitative regulation of FLC via coordinated transcriptional initiation and elongation. Proc Natl Acad Sci USA **113**: 218–223

Yang Y, Li L, Qu L-J (2016) Plant Mediator complex and its critical functions in transcription regulation. J Integr Plant Biol **58**: 106–118

Yoo CY, He J, Sang Q, Qiu Y, Long L, Kim RJ-A, Chong EG, Hahm J, Morffy N, Zhou P, et al. (2021) Direct photoresponsive inhibition of a p53-like transcription activation domain in PIF3 by Arabidopsis phytochrome B. Nat Commun **12**: 1–16

Zhang X, Yao J, Zhang Y, Sun Y, Mou Z (2013) The Arabidopsis Mediator complex subunits MED14/SWP and MED16/SFR6/IEN1 differentially regulate defense gene expression in plant immune responses. Plant J **75**: 484–497

Zhao H, Young N, Kalchschmidt J, Lieberman J, El Khattabi L, Casellas R, Asturias FJ (2021) Structure of mammalian Mediator complex reveals Tail module architecture and interaction with a conserved core. Nat Commun **12**: 1355

Zhu J-Y, Oh E, Wang T, Wang Z-Y (2016) TOC1–PIF4 interaction mediates the circadian gating of thermoresponsive growth in Arabidopsis. Nat Commun **7**: 13692